Research Square

Preprints are preliminary reports that have not undergone peer review.
They should not be considered conclusive, used to inform clinical practice,
or referenced by the media as validated information.

# Hyperelastic characterization of a cylinder under tension -- torsion

**MADAHAN BIEN--AIME LIMAN KAOYE**

limankaoylims@gmail.com

National School of Agro-Industrial Sciences, University of Ngaoundere

**Blaise BALE B.**

National School of Agro-Industrial Sciences, University of Ngaoundere

**GAMBO BETCHEWE**

Faculty of Sciences, University of Maroua

**Research Article**

**Keywords:** Poynting effect, Torsion, Tension–torsion, Hyperelasticity, Genetic algorithm

**Posted Date:** August 3rd, 2026

**DOI:** https://doi.org/10.21203/rs.3.rs-10512521/v1

**License:** This work is licensed under a Creative Commons Attribution 4.0 International License.
Read Full License

**Additional Declarations:** No competing interests reported.

# Hyperelastic characterization of a cylinder under tension – torsion

MADAHAN BIEN–AIME LIMAN KAOYE [1*],
Blaise BALE B. [1†], SAÏDJO[2†], GAMBO BETCHEWE[3†]

[1*]Department of Mechanical Engineering, National School of Agro-Industrial Sciences, University of Ngaoundere, Adamawa, Cameroon.
[2]University Institute of Technology, Laboratory of Simulations and Testings, University of Ngaoundere, Adamawa, Cameroon.
[3]Department of Physics, Faculty of Sciences, University of Maroua, Far North, Cameroon.

*Corresponding author(s). E-mail(s): limankaoylims@gmail.com;
Contributing authors: balebaidi.blaise@yahoo.com;
saidjbadou01@gmail.com; gambobetch@gmail.com;
†These authors contributed equally to this work.

**Abstract**

This work investigates the mechanical response of an incompressible hyperelastic cylinder subjected to pure torsion and combined tension–torsion loading. The constitutive behavior is described using the Pucci–Saccomandi model, which combines the Gent finite extensibility potential with a logarithmic term depending on the second invariant of the Cauchy–Green tensor. The formulation is developed in terms of principal stretches, allowing the derivation of general expressions for the stress components as well as the resultant quantities, namely the axial force and the torque.

The results reveal a pronounced strain-stiffening behavior under torsion, together with a strong coupling between axial stretch and twist. In particular, the model predicts the possibility of a reversal of the Poynting effect depending on the choice of material parameters. These findings highlight the ability of the proposed framework to capture complex nonlinear interactions in elastomeric materials under multiaxial loading.

The present study provides a consistent theoretical basis for the experimental identification of constitutive parameters from combined loading tests and offers

useful insights for the modeling and design of elastomeric structures subjected to coupled deformation modes.

**Keywords:** Poynting effect, Torsion, Tension–torsion, Hyperelasticity, Genetic algorithm

# 1 Introduction

Characterization and analysis of elastomers, and in particular rubber-like materials, constitute a cornerstone in numerous engineering applications, ranging from automotive [1–5] and aerospace industries [6] to biomedical engineering [5] and the design of vibration and damping systems [7–10]. These materials exhibit inherently nonlinear and highly complex mechanical responses, especially when subjected to large deformations, which require the development of robust hyperelastic constitutive models [1–3]. Such models are typically formulated in terms of a strain energy function, commonly denoted $W$ . The strain energy function may be expressed either as a function of the Cauchy–Green strain invariants $I_1$ and $I_2$ [3, 11, 12], or alternatively in terms of the main stretches $\lambda_i$ [13–16]. Conventional experimental protocols for characterizing hyperelastic behavior include uniaxial tension/compression, biaxial extension, and pure or simple shear [3, 16, 17]. Despite their widespread use, combined loading conditions such as simultaneous tension and torsion remain relatively underexplored, despite several earlier contributions [18–23]. This type of multiaxial loading gives rise to distinctive mechanical phenomena, most notably the Poynting effect, by which an axial extension emerges under conditions of pure torsion, as documented in several seminal works [6, 24–27]. Accurate analysis and prediction the response of elastomers under such combined loading conditions is of fundamental importance. Beyond advancing the scientific understanding of the constitutive behavior of elastomeric networks, such analysis are crucial for the informed selection, calibration, and validation of hyperelastic models employed in the engineering design of industrial components [1, 3, 4, 13]. A variety of hyperelastic strain energy functions have been proposed in the literature. Among them, the Gent model [28] has received particular attention due to its ability to capture the finite extensibility of polymer chains, thus providing a physically meaningful description of material behavior [29, 30]. Nevertheless, in order to enhance its predictive accuracy, several recent studies have advocated the inclusion of corrective terms involving the second invariant $I_2$ [3, 31]. Such extensions improve the model's ability to simultaneously reproduce distinct deformation modes under large strains [5, 11, 32]. In this context, the present work focuses on the mechanical characterization of a rubber cylinder subjected to combined tension–torsion loading. The hyperelastic parameters of the selected constitutive model are identified using a metaheuristic optimization procedure based on the genetic algorithm [3, 7, 14, 22, 33, 34]. The predictive performance of the model is subsequently evaluated through direct comparison with the experimental data of Rivlin [18, 35], thereby assessing its ability to accurately reproduce both torsional responses and the axial force component associated with the Poynting effect [17, 23, 27, 36–38].

# 2 Governing equations for a rubber-like cylinder under extension–torsion

## 2.1 Kinematics of torsion

In the study of a cylinder subjected to combined extension and torsion, the classical formulation introduced by Rivlin and Saunders [27, 37, 39–43] provides the fundamental equations, which are recalled here for completeness. Fig. 1 illustrates the notation adopted to describe both the reference and the deformed configurations of a homogeneous cylinder under simultaneous tension and torsion. Rubber-like materials are generally considered incompressible [26], and the deformation is therefore assumed to be isochoric [3, 4]. On this basis, the general analytical framework of the torsion problem is established and will serve as the foundation for the subsequent global analysis. In the cylindrical coordinate system $(\vec{u}_\rho, \vec{u}_\theta, \vec{u}_z)$, a material point $M$ in the

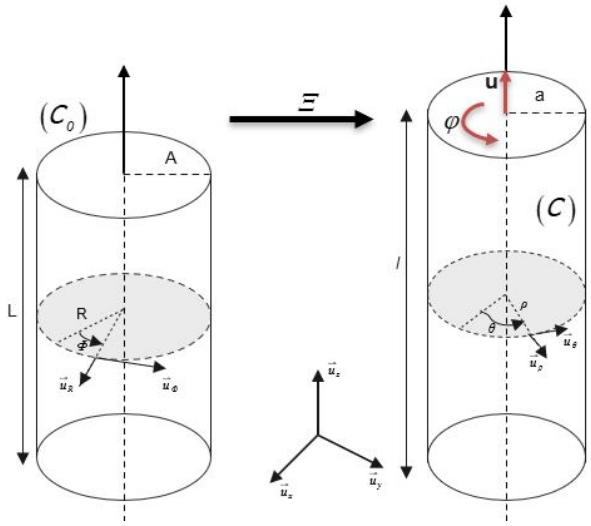



**Fig. 1** Kinematics of a cylindrical specimen under tension–torsion loading

reference configuration is defined by its coordinates $(R, \Theta, Z)$. Its deformed counterpart, denoted by $P$, is described by the coordinates $(\rho, \theta, z)$. The imposed uniaxial deformation consists of two components:

- an axial displacement $u$ along the $z$-axis,
- a twist angle $\varphi$ about the same axis.

Following Rivlin and Saunders [35], the deformation mapping for an incompressible cylinder subjected to combined tension and torsion is written as follows

$$(\rho, \theta, z) = \left( \frac{R}{\sqrt{\lambda}},\ \Theta + \lambda\, \psi\, Z,\ \lambda\, Z \right), \tag{1}$$

where the axial stretch ratio $\lambda$ and the twist per unit of reference length $\psi$ are defined by

$$\lambda = \frac{l}{L}, \qquad \psi = \frac{\varphi}{L}. \tag{2}$$

With respect to the orthogonal basis $(\vec{u}_R, \vec{u}_\Theta, \vec{u}_Z)$ in the reference configuration and $(\vec{u}_\rho, \vec{u}_\theta, \vec{u}_z)$ in the current configuration, the deformation gradient takes the form of

$$\mathbf{F} = \frac{1}{\sqrt{\lambda}} \left(u_r \otimes u_R + u_\theta \otimes u_\Theta\right) + \sqrt{\lambda}\, \psi R\, u_\theta \otimes u_Z + \lambda\, u_z \otimes u_Z \tag{3}$$

Based on Eq. (3), the Cauchy-Green strain tensor $\mathbf{C}$ can be expressed by the following equation [43, 44] :

$$\begin{aligned} \mathbf{C} = \mathbf{F}^{\mathsf{T}}\mathbf{F} = \frac{1}{\lambda}\, u_R \otimes u_R + \frac{1}{\lambda}\, u_\Theta \otimes u_\Theta \\ + \lambda\psi^2 R^2\, u_\Theta \otimes u_\Theta + \lambda^2\, u_Z \otimes u_Z \\ + \lambda\psi R \left(u_\Theta \otimes u_Z + u_Z \otimes u_\Theta\right). \end{aligned} \tag{4}$$

The present analysis is restricted to homogeneous, incompressible, isotropic hyperelastic materials. For these materials, the constitutive response is determined by a strain energy function $W$, which, for isotropic solids, is a function of the first two invariants of the right Cauchy–Green tensor $\mathbf{C}$, denoted $I_1$ and $I_2$, and defined by [3, 45] :

$$\begin{aligned} I_1 &= \mathrm{tr}(\mathbf{C}), \\ I_2 &= \frac{1}{2}\Big[(\mathrm{tr}\mathbf{C})^2 - \mathrm{tr}(\mathbf{C}^2)\Big]. \end{aligned} \tag{5}$$

Using the right Cauchy–Green deformation tensor $\mathbf{C}$ (Eq. (3)), the first and second invariants take the form [56,43] :

$$\begin{aligned} I_1 &= \psi^2\rho^2 + \frac{2}{\lambda} + \lambda^2, \\ I_2 &= \frac{\psi^2\rho^2}{\lambda} + \frac{1}{\lambda^2} + 2\lambda. \end{aligned} \tag{6}$$

In order to determine the Cauchy stress $\sigma$, it is necessary to evaluate the inverse of the tensor $\mathbf{C}$, which can be expressed as follows :

$$\begin{aligned} \mathbf{C}^{-1} = \mathbf{F}^{-1}\mathbf{F}^{-\mathsf{T}} = \lambda\, \mathbf{u}_\rho \otimes \mathbf{u}_\rho + \frac{1}{1+\lambda^3\psi^2R^2}\Bigg[\lambda^2\, \mathbf{u}_\theta \otimes \mathbf{u}_\theta \\ + \frac{1+\lambda^4\psi^2R^2}{\lambda}\, \mathbf{u}_z \otimes \mathbf{u}_z - \lambda\psi R \left(\mathbf{u}_\theta \otimes \mathbf{u}_z + \mathbf{u}_z \otimes \mathbf{u}_\theta\right)\Bigg] \end{aligned} \tag{7}$$

In the reference configuration, using Eqs. (3) and (7) the Cauchy stress can be written as:

$$\sigma = \frac{1}{J}\,\mathbf{F}\left(-p\,\mathbf{C}^{-1} + 2\frac{\partial W}{\partial I_1}\,\mathbf{I} - 2\frac{\partial W}{\partial I_2}\,\mathbf{C}\right)\mathbf{F}^T, \quad J = \det\mathbf{F} \tag{8}$$

$$\sigma = -p\,\mathbf{I} + 2\frac{\partial W}{\partial I_1}\,\mathbf{B} - 2\frac{\partial W}{\partial I_2}\,\mathbf{B}^{-1} \tag{9}$$

With the left Cauchy–Green deformation tensor $\mathbf{B}$, defined as admitting the following tonsorial representation :

$$\mathbf{B} = \frac{1}{\lambda}\,u_\rho \otimes u_\rho + \left(\frac{1}{\lambda} + \lambda\psi^2 R^2\right) u_\theta \otimes u_\theta + \lambda^2\,u_z \otimes u_z + \lambda\psi R\,(u_\theta \otimes u_z + u_z \otimes u_\theta) \tag{10}$$

And The inverse of the tensor $\mathbf{B}$ can be in dyadic form as follows :

$$\mathbf{B}^{-1} = \lambda\,u_\rho \otimes u_\rho + \frac{1}{1+\lambda^3\psi^2R^2}\left(\lambda^2\,u_\theta \otimes u_\theta + \frac{1+\lambda^4\psi^2R^2}{\lambda}\,u_z \otimes u_z - \lambda\psi R\,(u_\theta \otimes u_z + u_z \otimes u_\theta)\right) \tag{11}$$

Alternatively, Cauchy stress can be expressed in the following form :

$$\begin{aligned}\boldsymbol{\sigma}(\rho) = {} & \left(2\frac{\partial W}{\partial I_1}\lambda^{-1} - 2\frac{\partial W}{\partial I_2}\lambda - p\right)\,\mathbf{u}_\rho \otimes \mathbf{u}_\rho + \left(2\frac{\partial W}{\partial I_1}\left(\lambda^{-1} + \psi^2\rho^2\right) - 2\frac{\partial W}{\partial I_2}\lambda - p\right)\,\mathbf{u}_\theta \otimes \mathbf{u}_\theta \\ & + \left(2\frac{\partial W}{\partial I_1}\lambda^2 - 2\frac{\partial W}{\partial I_2}\left(\lambda^{-2} + \tfrac{\psi^2\rho^2}{\lambda}\right) - p\right)\,\mathbf{u}_z \otimes \mathbf{u}_z + \psi\rho\left(2\frac{\partial W}{\partial I_1}\lambda + 2\frac{\partial W}{\partial I_2}\right)\,(\mathbf{u}_\theta \otimes \mathbf{u}_z + \mathbf{u}_z \otimes \mathbf{u}_\theta)\end{aligned} \tag{12}$$

Using Eq. (12), the hydrostatic pressure $p$ is determined from the equilibrium equation in the radial direction, which takes the form of :

$$\frac{d\sigma_{11}}{d\rho} + \frac{1}{\rho}\,(\sigma_{11} - \sigma_{22}) = 0, \quad 0 < \rho < a. \tag{13}$$

Integration of Eq. (13) from the inner radius $\rho = a$ to the lateral surface, combined with the constitutive relations and the boundary condition, provides the expression of $p$ at $\rho$ [22]. Next, attention is directed to the description of the stress state, with the aim of deriving the Cauchy stress tensor $\sigma$. Within the theoretical framework, the axial force $N$ and the torque $M$ are determined by integrating the constitutive equations under the prescribed boundary conditions.
The total axial force is defined by :

$$N = \int_S \sigma_{33}(\rho)\,dS = 2\pi\int_0^a \sigma_{33}(\rho)\,\rho\,d\rho \tag{14}$$

Taking into account the contribution of the invariants and the radial integral, the axial Cauchy stress $\sigma_{33}(\rho)$ takes the form :

$$\sigma_{33}(\rho) = 2\frac{\partial W}{\partial I_1}(\rho)\ \left(\lambda^2 - \lambda^{-1}\right) - 2\frac{\partial W}{\partial I_2}(\rho)\left(\lambda^2 - \lambda^{-1} + \frac{\psi^2\rho^2}{\lambda}\right) - 2\psi^2\int_\rho^a \frac{\partial W}{\partial I_1}(s)\, s\, ds \tag{15}$$

1. The first term $2\,\frac{\partial W}{\partial I_1}(\rho)(\lambda^2 - \lambda^{-1})$ represents the contribution of the first invariant, associated with the axial stretch.
2. The second term $-2\frac{\partial W}{\partial I_2}(\rho)\left(\lambda^2 - \lambda^{-1} + \frac{\psi^2\rho^2}{\lambda}\right)$ corresponds to the influence of the second invariant, including the torsional effect.
3. The last term $-2\psi^2\int_\rho^a W_1(s)\, s\, ds$ reflects the radial integral contribution, which accounts for the distribution of the strain–energy density $W$ associated with the first invariant $I_1$ across the thickness of the wall.

## 2.2 Resultant torsional moment and axial force

The objective is to obtain the analytical expressions of $N$ and $M$, corresponding to the axial force and the torque, respectively.
Substituting the relation (15) into the integral yields :

$$N = 2\pi\int_0^a \left[2\frac{\partial W}{\partial I_1}(\rho)(\lambda^2 - \lambda^{-1}) - 2\frac{\partial W}{\partial I_2}(\rho)\left(\lambda^2 - \lambda^{-1} + \frac{\psi^2\rho^2}{\lambda}\right) - 2\psi^2\int_\rho^a \frac{\partial W}{\partial I_1}(s) s\, ds\right]\rho\, d\rho \tag{16}$$

Rearranging the terms, it follows that :

$$N = 4\pi\left(\lambda - \lambda^{-2}\right)\int_0^a \left(\lambda\frac{\partial W}{\partial I_1}(\rho) + \frac{\partial W}{\partial I_2}(\rho)\right)\rho\, d\rho - \frac{4\pi\psi^2}{\lambda}\int_0^a \frac{\partial W}{\partial I_2}(\rho)\rho^3\, d\rho - 4\pi\psi^2\int_0^a \rho\int_\rho^a \frac{\partial W}{\partial I_1}(s) s\, ds\, d\rho \tag{17}$$

According to Fubini's theorem, the last term in Eq. (17), denoted $N_3$, can be rewritten by interchanging the order of integration as follows :

$$N_3 = \int_0^a \left(\int_0^s \rho\, d\rho\right)\frac{\partial W}{\partial I_1}(s)\, s\, ds = \frac{1}{2}\int_0^a \frac{\partial W}{\partial I_1}(s)\, s^3\, ds, \tag{18}$$

where the inner radial integration is kept in a formal form, showing that the contribution of $I_1$ to the axial force follows the radial distribution.
Consequently, the total axial force $N$ for a hyperelastic cylinder under combined axial stretch $\lambda$ and torsion $\psi$ reads [18] :

$$N = 4\pi(\lambda - \lambda^{-2})\int_0^a \left(\frac{\partial W}{\partial I_1} + \frac{1}{\lambda}\frac{\partial W}{\partial I_2}\right)\rho\, d\rho - 2\pi\psi^2\int_0^a \left(\frac{\partial W}{\partial I_1} + \frac{2}{\lambda}\frac{\partial W}{\partial I_2}\right)\rho^3\, d\rho. \tag{19}$$

Here, the first integral corresponds to the contribution of axial stretching, linearly weighted with the radial coordinate $\rho$, while the second integral accounts for the

torsional effect, which introduces a cubic radial weight due to the deformation distribution across the cylinder section. Finally, $\frac{\partial W}{\partial I_1}$ and $\frac{\partial W}{\partial I_2}$ represent the material response functions derived from the chosen hyperelastic strain-energy density $W(I_1, I_2)$.
Regarding the expression of torque $M$, it is defined as the integral of the shear stress component $\sigma_{23}$ in the cross-sectional area $S$ of the cylinder:

$$M = \int_S \rho\, \sigma_{23}\, dS = \int_0^{2\pi} \int_0^a \rho\, \sigma_{23}\, \rho\, d\rho\, d\theta = 2\pi \int_0^a \rho^2\, \sigma_{23}\, d\rho \tag{20}$$

Here, $\rho$ denotes the radial coordinate in the cylindrical section. The factor $\rho$ inside the integrals accounts for the moment arm relative to the rotation axis, while the conversion to polar coordinates introduces the factor $2\pi\rho$ from the element of area $dS = 2\pi\rho\, d\rho$. This formulation emphasizes that torque is generated by the distribution of shear stress weighted by the radial distance, emphasizing the contribution of the outer fibers of the cylinder to the total moment.
According to Eq. (12), the shear stress component $\sigma_{23}$ in the cylinder under combined axial stretch and torsion can be expressed as :

$$\sigma_{23} = 2\,\psi\,\rho \left(\lambda \frac{\partial W}{\partial I_1} + \frac{\partial W}{\partial I_2}\right), \tag{21}$$

By substituting Eq. (21) into the definition of the torque $M$, Eq. (20) and performing the necessary simplifications, one obtains the final expression of $M$ as [46] :

$$M = 4\pi\,\psi \int_0^a \left(\frac{\partial W}{\partial I_1} + \frac{1}{\lambda}\frac{\partial W}{\partial I_2}\right) \rho^3\, d\rho \tag{22}$$

In summary, the axial force $N$ and torque $M$ are determined by the derivatives of the strain-energy function with respect to the invariants, integrated over the cylinder's cross-section. $N$ reflects both both axial stretch and torsion effects with linear and cubic radial weighting, while $M$ is dominated by the outer fibers due to its cubic radial dependence, providing a clear basis for the analytical and numerical evaluation of the hyperelastic response cylinder under combined loading.

# 3 Hyperelastic constitutive models for cylinders under torsion

For incompressible isotropic materials, the strain-energy density $W$ is a function of the invariants $I_1$ and $I_2$ of the Cauchy-Green tensor (Eqs. (5) and (6)), which themselves depend on the radial coordinate $\rho$, the torsion rate $\psi$, and the axial stretch $\lambda$. In the literature, a wide range of hyperelastic models have been proposed to describe the mechanical response of rubber-like materials, particularly under the fundamental loading modes of uniaxial tension, equibiaxial extension, and shear[1, 2, 6]. In the specific case of torsion, the formulations most frequently employed are the Neo-Hookean and Mooney–Rivlin models [25, 35, 37, 41]. However, in order to better capture the

nonlinear effects observed experimentally while maintaining relative simplicity, the present work focuses on models derived from the Gent formulation [28, 47, 48].

### 3.1 Gent model

The Gent model [28, 47], in particular, represents an attractive alternative due to its limited number of material parameters and its ability to account for moderate nonlinearities while still reproducing the essential mechanical behavior of elastomers. The associated strain-energy density function is expressed as :

$$W(I_1) = -\frac{\mu\, J_m}{2}\, \ln\left(1 - \frac{I_1 - 3}{J_m}\right) \tag{23}$$

where $\mu$ is the initial shear modulus, characterizing the stiffness of the material, and $J_m$ is the extensibility limiting chain, representing the maximum allowable stretch of the polymer network.

### 3.2 Pucci–Saccomandi hyperelastic model

The Pucci–Saccomandi model [30] was developed as an extension of the classical Gent model, which has difficulty accurately reproducing the biaxial extension behavior observed in Treloar's experimental data [17], the most widely used dataset in the literature [1, 5, 12, 13, 15, 16, 32, 45]. Although the additional logarithmic term in $I_2$, weighted by the parameter $K$, allows the model to satisfy various criteria for large deformations,it still fails to accurately describe the biaxial extension behavior observed in Treloar's experiments [17]. The strain-energy density function can be written as :

$$W_{PC}(I_1, I_2) = -\frac{\mu\, J_m}{2}\, \ln\left(1 - \frac{I_1 - 3}{J_m}\right) + K \ln\left(\frac{I_2}{3}\right) \tag{24}$$

### 3.3 Liman et *al.*, strain energy model

Liman et *al.*, [3] revisited the models of Gent [48] and Pucci–Saccomandi [30] by introducing a square-root dependency in the term $I_2$ to improve the prediction of the biaxial response. Their strain-energy function is given by :

$$W_L(I_1, I_2) = K\left(I_2^{-1/2} - 3^{-1/2}\right) - \frac{\mu\, J_m}{2}\, \ln\left(1 - \frac{I_1 - 3}{J_m}\right) \tag{25}$$

For an unextended cylinder, for $\lambda = 1$, the axial force $N$ given by Eq. (19) can be expressed as :

$$N = -2\pi\, \psi^2 \int_0^a \left(\frac{\partial W}{\partial I_1} + 2\frac{\partial W}{\partial I_2}\right) \rho^3\, d\rho \tag{26}$$

The torque $M$ is obtained from Eq. (20) :

$$M = 4\pi\, \psi \int_0^a \left(\frac{\partial W}{\partial I_1} + \frac{\partial W}{\partial I_2}\right) \rho^3\, d\rho \tag{27}$$

The corresponding expressions for the deformation invariants simplify to :

$$I_1 = I_2 = \psi^2 \rho^2 + 3 \tag{28}$$

Following the classical studies of Rivlin and Saunders [35], it is established that, to impose a magnitude torsion $\psi$ on a right-circular rubber cylinder with flat rigidly constrained ends, a torque $M$ along with an axial force $-N$ must be applied at the ends of the cylinder [35, 43, 44].

# 4 Analysis of axial force and torsional moment as stress resultants

Considering the strain-energy functions defined by Eqs. (25) and (24) and performing a fourth-order truncated expansion of the torsional moment $M$ and axial force $N$, the resulting expressions for the first model are :

$$\begin{aligned} M_{PC}(\psi) &= \pi a^4 \left(\frac{\mu}{2} + \frac{K}{3}\right)\psi + \frac{2\pi a^6}{3}\left(\frac{\mu}{2J_m} - \frac{K}{9}\right)\psi^3, \\ -N_{PC}(\psi) &= \pi a^4 \left(\frac{\mu}{4} + \frac{K}{3}\right)\psi^2 + \frac{\pi a^6}{3}\left(\frac{\mu}{2J_m} - \frac{2K}{9}\right)\psi^4 \end{aligned} \tag{29}$$

For the second model, the corresponding expressions, also truncated at fourth order, are :

$$\begin{aligned} M_{L}(\psi) &= \pi a^4 \left(\frac{\mu}{2} + \frac{K}{2\sqrt{3}}\right)\psi + \frac{\pi a^6}{3}\left(\frac{\mu}{J_m} - \frac{K}{6\sqrt{3}}\right)\psi^3, \\ -N_{L}(\psi) &= \frac{\pi a^4}{2}\left(\frac{\mu}{2} + \frac{K}{\sqrt{3}}\right)\psi^2 + \frac{\pi a^6}{3}\left(\frac{\mu}{2J_m} - \frac{K}{6\sqrt{3}}\right)\psi^4 \end{aligned} \tag{30}$$

# 5 Genetic algorithm for hyperelastic material parameter identification

In the present study, a genetic algorithm (GA) is used to identify the parameters of hyperelastic constitutive models using experimental data on the torsion of Rivlin and Saunders [35], which remain a widely recognized benchmark for rubber-like materials under torsional loading. Torsion tests provide a particularly stringent framework for model validation, as they involve coupled stress components and large deformations, making the mechanical response highly sensitive to the specific form of the strain-energy density function. Inspired by the principles of natural selection and genetic evolution, genetic algorithms are designed to identify global optima without requiring explicit prior knowledge of the problem structure. The procedure begins with the generation of an initial population composed of candidate solutions, referred to as individuals or chromosomes [3, 14, 33, 49]. Each individual is then evaluated using a predefined objective function to assess its fitness. Based on these evaluations, a

**Table 1** Optimal hyperelastic parameters identified from the Rivlin–Saunders experimental data [35]

| Parameter | Liman *et al.* | Pucci–Saccomandi |
|---|---|---|
| $\mu$ | $1.700 \times 10^{-3}$ | $8.600 \times 10^{-3}$ |
| $J_m$ | $5.600 \times 10^{-3}$ | $2.860 \times 10^{-2}$ |
| $K$ | $4.800 \times 10^{-3}$ | $3.853 \times 10^{-4}$ |

subset of individuals is selected as parents according to a given selection strategy. This evolutionary process is repeated until a convergence criterion is satisfied, typically characterized by a stabilization of the populations genetic structure or negligible improvement in fitness values. At this stage, individuals in the population exhibit similar performance levels, indicating that the algorithm has converged toward an optimal or near-optimal solution [35, 43, 44]. The objective of this study is to formulate and solve a parametric optimization problem aimed at identifying the set of constitutive parameters that best fits the experimental data. Within the framework of a hyperelastic model under torsion, the parameters are determined by minimizing the mean squared error $\chi$ (Eq. 31), which quantifies the discrepancy between the analytical predictions of the model and the experimental measurements reported by Rivlin and Saunders [35]. The objective function, which quantifies the discrepancy between experimental observations and model predictions, is defined as follows [3, 4, 22, 49, 50] :

$$\chi = \sum_{i=1}^{N} \left[\sigma_i^{\exp} - \sigma_i(\theta)\right]^2 \tag{31}$$

where $\sigma^{\exp}$ denotes the experimental response, $\sigma(\theta)$ the analytical or numerical prediction, and $\theta$ the set of parameters the hyperelastic material.

# 6 Results and Discussion

Figure 2 presents a comparison between the experimental data of Rivlin–Saunders and the predictions of the hyperelastic models of Pucci–Saccomandi and Liman *et al.* : (a) the torsional moment $M$ as a function of the angle of twist $\psi$, and (b) the normal force $N$ as a function of $\psi^2$. In Fig. 2(a), both models exhibit excellent agreement with the experimental data throughout the deformation range. The predicted curves are nearly indistinguishable and closely follow the quasi-linear trend observed experimentally, indicating that both formulations accurately capture the torsional response. Minor deviations may be observed at intermediate values of $\psi$, where the experimental data exhibit a slightly higher slope. However, these differences remain negligible and do not significantly affect the overall predictive capacity. In Fig. 2(b), the normal force $N$ is also well captured by both models, with predictions closely matching the experimental data across the full range of $\psi^2$. Nevertheless, small discrepancies become more pronounced at higher deformation levels. In particular, the Pucci–Saccomandi model tends to slightly overestimate the response, whereas the Liman *et al.* model remains in closer agreement with the experimental measurements. This suggests that the latter

provides a more accurate representation of the nonlinear coupling effects governing the normal force. Overall, both models demonstrate a high level of accuracy in reproducing the experimental behavior, which confirms their suitability for describing the torsion of hyperelastic materials. However, the Liman *et al.* model shows a marginally improved predictive performance, particularly for the normal force, which is more sensitive to nonlinear deformation mechanisms. Figures 2(a) and (b) also illustrate the

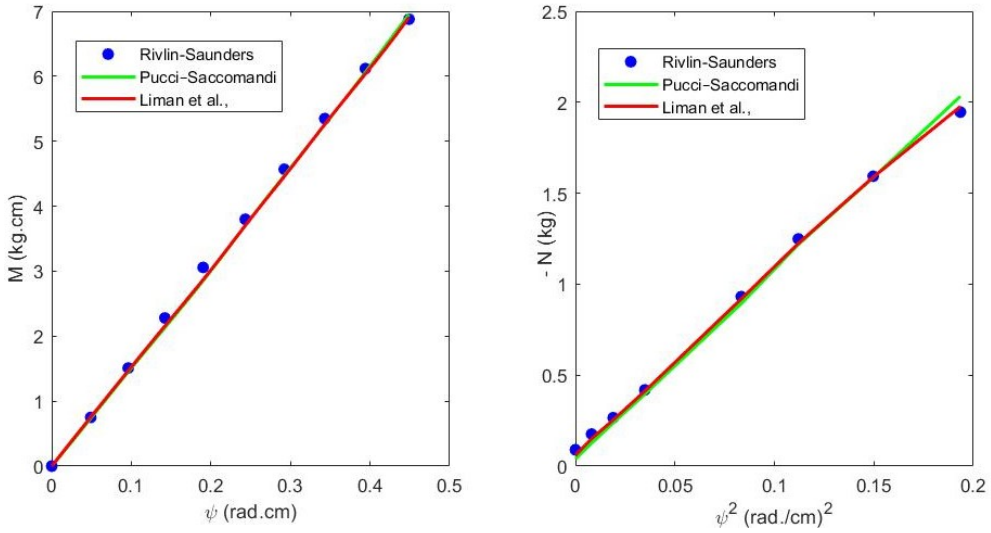



**Fig. 2** Comparison of hyperelastic model predictions: (a) torsional moment $M$ versus angle of twist $\psi$; (b) normal force $N$ versus $\psi^2$.

local relative error between the Rivlin–Saunders experimental data and the predictions of the Pucci–Saccomandi and Liman *et al.* models for the torsional moment $M$ and the normal force $N$, respectively. For the torsional moment $M$ (Fig. 2(a)), both models exhibit excellent agreement with the experimental response, as reflected by very high coefficients of determination ($R^2 > 0.999$). The relative error remains negligible at both both small and large twist angles, while a pronounced peak appears in the intermediate range ($\psi \approx 0.15$–$0.20$ rad), highlighting the difficulty of accurately capturing the nonlinear transition of the response material. Quantitatively, the Liman *et al.* model outperforms the Pucci–Saccomandi model, as indicated by lower error metrics (RMSE = 0.0201 vs 0.0342; MAE = 0.0139 vs 0.0222), suggesting a more accurate representation of the dominant contribution of the first invariant $I_1$ under torsional loading. For the normal force $N$ (Fig. 2(b)), the discrepancy between the models becomes more significant. The relative error increases up to a maximum around $\psi^2 \approx 0.08$, followed by a monotonic decrease at larger deformations. The Pucci–Saccomandi model exhibits noticeably larger deviations over a wide deformation range [30], while the Liman *et al.* model provides a substantially improved fit [3]. This is confirmed by the statistical indicators (RMSE = 0.0208 vs 0.0451; MAE

= 0.0184 vs 0.0392; $R^2 = 0.9990$ vs 0.9953). This improvement can be attributed to a more effective representation of the coupling between the invariants $I_1$ and $I_2$, which plays a crucial role in capturing the normal force response. This response is known to be highly sensitive to hydrostatic effects and nonlinear deformation mechanisms. In summary, although both models successfully reproduce the main experimental trends, the formulation of Liman *et al.* demonstrates superior accuracy and robustness across the entire deformation range, particularly in predicting the normal force, which constitutes a more stringent test for hyperelastic constitutive models.

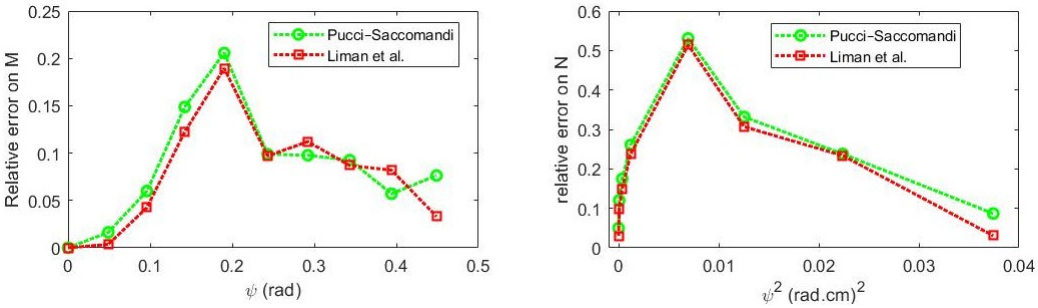



**Fig. 3** Local relative error between experimental data and hyperelastic model predictions for (a) torsional moment $M$ and (b) normal force $N$.

# 7 Poynting effect in finite torsion of a hyperelastic cylinder

## 7.1 Kinematic framework

An incompressible hyperelastic cylinder of undeformed radius $R$ is subjected to a combined deformation that involves a finite axial elongation $\lambda$ and a finite angle of twist per unit length $\psi$. Under these conditions, the first two principal invariants of the left Cauchy–Green deformation tensor can be expressed as [1, 19, 31, 44, 50, 51] :

$$I_1 = \lambda^2 + \frac{2}{\lambda} + \psi^2\rho^2 \quad \text{and} \quad I_2 = 2\lambda + \frac{1}{\lambda^2} + \psi^2\rho^2 \tag{32}$$

Taking into account the strain energy density functions introduced in Eqs. (29) and (30), the axial force $N(\psi, \lambda)$ associated with each constitutive model, respectively, is governed by the following expressions at $\psi = 0$ :

$$N^{(0)}(\lambda) = \frac{\pi a^2(\lambda^3 - 1)}{\lambda}\left[\frac{\mu(J_m - 3)}{P} + \frac{2K}{Q}\right] \tag{33a}$$

$$N^{(2)}(\lambda) = \pi a^4\lambda^2\left[\frac{\mu(J_m - 3)(3\lambda^2 - J_m)}{4P^2} - \frac{3K\lambda^2}{Q^2}\right] \tag{33b}$$

$$N^{(4)}(\lambda) = \pi a^6 \lambda^4 \left[ \frac{\mu(J_m - 3)(3\lambda^2 - J_m)}{6P^3} + \frac{2K\lambda^2}{Q^3} \right] \tag{33c}$$

$$P = \lambda J_m - \lambda^3 - 2, \qquad Q = 2\lambda^3 + 1 \tag{34}$$

Substituting Eqs. (33a)–(33c) into the general expansion, the complete expression of the axial force for model $W_2$ reads :

$$N_{PS}(\psi, \lambda) = N^{(0)}(\lambda) + N^{(2)}(\lambda)\,\psi^2 + N^{(4)}(\lambda)\,\psi^4 \tag{35}$$

Following the same procedure, substitution of the auxiliary quantities $P$ and $Q$, as defined in Eq. (34), into the general expansion leads to the three coefficients of the axial force associated with model $W_L$ :

$$N^{(0)}(\lambda) = \frac{\pi a^2(\lambda^3 - 1)}{\lambda} \left[ \frac{\mu(J_m - 3)}{P} + K\,Q^{-1/2} \right] \tag{36a}$$

$$N^{(2)}(\lambda) = \pi a^4 \lambda^2 \left[ \frac{\mu(J_m - 3)(3\lambda^2 - J_m)}{4P^2} - \frac{3}{4} K\,Q^{-3/2} \right] \tag{36b}$$

$$N^{(4)}(\lambda) = \pi a^6 \lambda^4 \left[ \frac{\mu(J_m - 3)(3\lambda^2 - J_m)}{6P^3} + \frac{15}{8} K\,Q^{-5/2} \right] \tag{36c}$$

Using Eqs. (36a) – (36c), the expression of the axial force $N_L$ for the model reads :

$$N_L(\psi, \lambda) = N^{(0)}(\lambda) + N^{(2)}(\lambda)\,\psi^2 + N^{(4)}(\lambda)\,\psi^4 \tag{37}$$

The variation of the normal force $N$ as a function of $\psi$ and $\lambda$ is analyzed for models 29 and 30, using the hyperelastic parameters provided in Table 1. The corresponding results are presented in Figs. 4 and 5, respectively. These results reveal a pronounced nonlinear increase of $N$ with $\psi$, together with a marked amplification effect induced by increasing values of $\lambda$. Fig. 6 highlights the evolution of the normal force $N$ as a function of $\psi$ for different values of $\lambda$. A nonlinear increase of $N$ is observed in all cases, with a more pronounced effect at high levels of deformation. Increasing $\lambda$ leads to a significant amplification of the response, reflecting the expected stretch-induced stiffening effect. A systematic discrepancy between the two models is also evident: the $N_L$ model predicts higher values than $N_{PS}$, particularly for large values of $\psi$. This trend is in better agreement with the experimental observations, suggesting that the $N_L$ model provides a more accurate representation of mechanical behavior, while $N_{PS}$ tends to underestimate the response at high levels of deformation. This observation is consistent with the error curve shown in Fig. 6, which further confirms the superior predictive accuracy of the model $N_L$.

# 8 Conclusion

This work has presented a detailed analytical and numerical study of the mechanical response of an incompressible hyperelastic cylinder subjected to pure torsion and

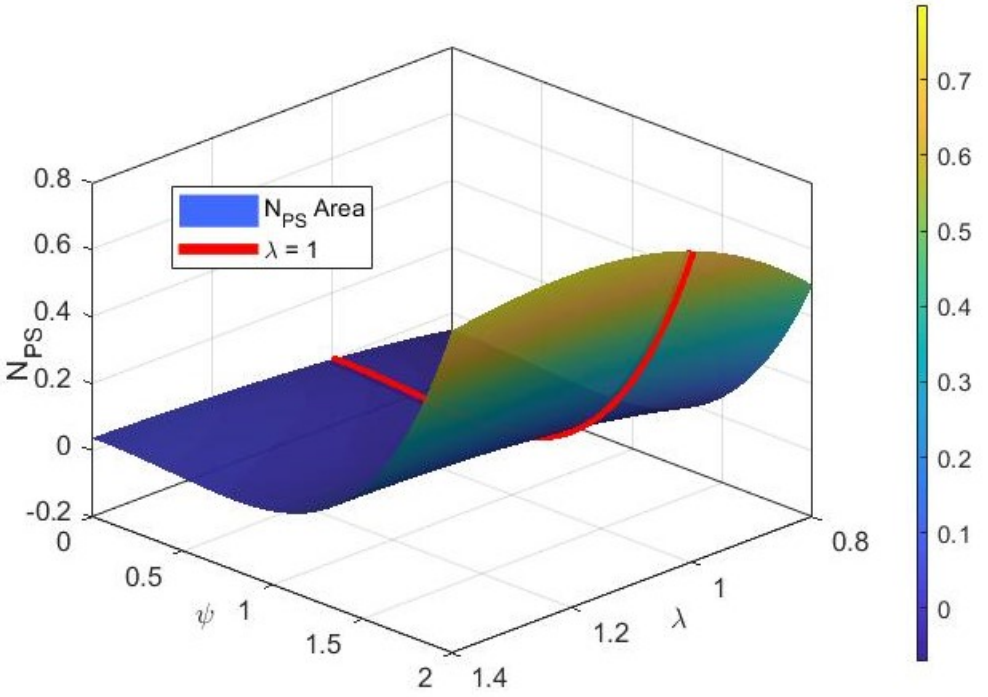



**Fig. 4** Variation of the normal force $N(\psi, \lambda)$ for the Pucci–Saccomandi model, highlighting the Poynting effect

combined finite tension–torsion, with particular emphasis on the Poynting effect. The analysis relies on two constitutive models, namely those of Pucci–Saccomandi [30] and Liman *et al.* [3]. Both formulations incorporate the finite extensibility constraint through a logarithmic dependence on the first invariant $I_1$, while differing exclusively in the functional form adopted for the second invariant $I_2$ : logarithmic in the former and of power-law type in the latter. This distinction enables a direct assessment of the influence of $I_2$ on the axial response. In the case of pure torsion, analytical expressions for the torsional moment $M$ and the axial force $N$ were derived using a Taylor expansion with respect to the twist angle $\psi$. The material parameters $(\mu, J_m, K)$ were identified by using a genetic algorithm method, ensuring robust convergence despite the non-convex nature of the optimization problem. Both models accurately reproduce the experimental torsional response reported by Rivlin–Saunders [35]. However, significant differences arise in the prediction of the axial force : the Liman *et al.* model provides a more accurate description of the normal force, as evidenced by consistently lower residual errors, indicating an improved representation of the coupling between $I_1$ and $I_2$. The analysis was subsequently extended to the combined tension–torsion configuration. The general expressions for the Cauchy stress tensor and the resulting axial force $N(\psi, \lambda)$ were established within the framework of finite kinematics. The resulting decomposition shows that both models share an identical contribution associated with $I_1$, while their differences originate only from the terms that involve $I_2$. These terms exhibit distinct algebraic structures in each model, providing a clear basis for identifying their respective roles in the nonlinear axial response. The numerical results demonstrate that axial elongation $\lambda$ plays a

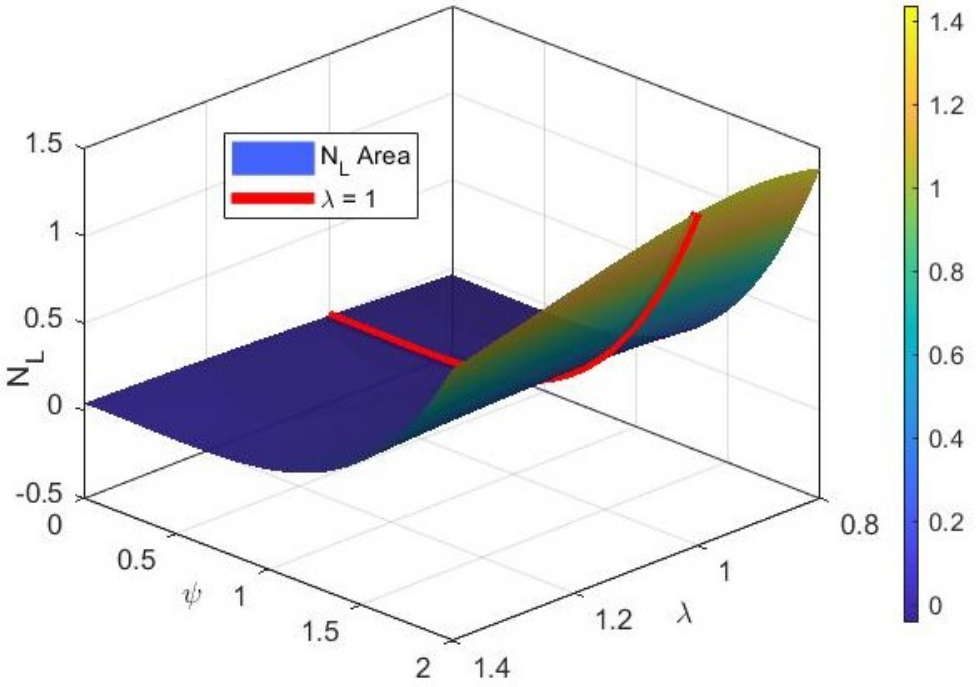



**Fig. 5** Variation of the normal force $N(\psi, \lambda)$ for the Liman *et al.*, model, highlighting the Poynting effect

dominant role in the amplification of the Poynting effect. An increase in $\lambda$ leads to a marked increase in the axial force $N$, reflecting the progressive stiffening of the material under combined loading. The dependence of $N$ on the twist angle $\psi$ is strongly nonlinear and is well captured by the adopted asymptotic approximation. A systematic discrepancy between the two models is observed at large deformation levels : the Liman *et al.* model predicts higher axial forces, in closer agreement with experimental observations, whereas the Pucci–Saccomandi model tends to underestimate the response. This difference is directly attributable to the functional form of the $I_2$-dependent contribution, highlighting the relevance of the power-law formulation in capturing nonlinear coupling effects. In general, the present results emphasize the critical role of the second invariant $I_2$ in the constitutive modeling of elastomeric materials subjected to finite multiaxial deformations. The proposed framework provides both a consistent analytical basis and a useful benchmark for the comparative assessment of hyperelastic models under combined loading conditions. Future developments may include the extension of this framework to other hyperelastic models, such as Ogden [52] or Arruda–Boyce [53], as well as the incorporation of additional physical effects, including viscoelasticity, Mullins-type softening [31, 35, 54], and anisotropy. From a structural perspective, extensions to more complex geometries, such as thick-walled or hollow cylinders, constitute a natural direction [8, 55–57]. Further experimental investigations under multiaxial loading conditions would also be valuable to strengthen and consolidate the present conclusions.

**Acknowledgements**
The authors declare that they have no known competing financial interests or personal relationships that

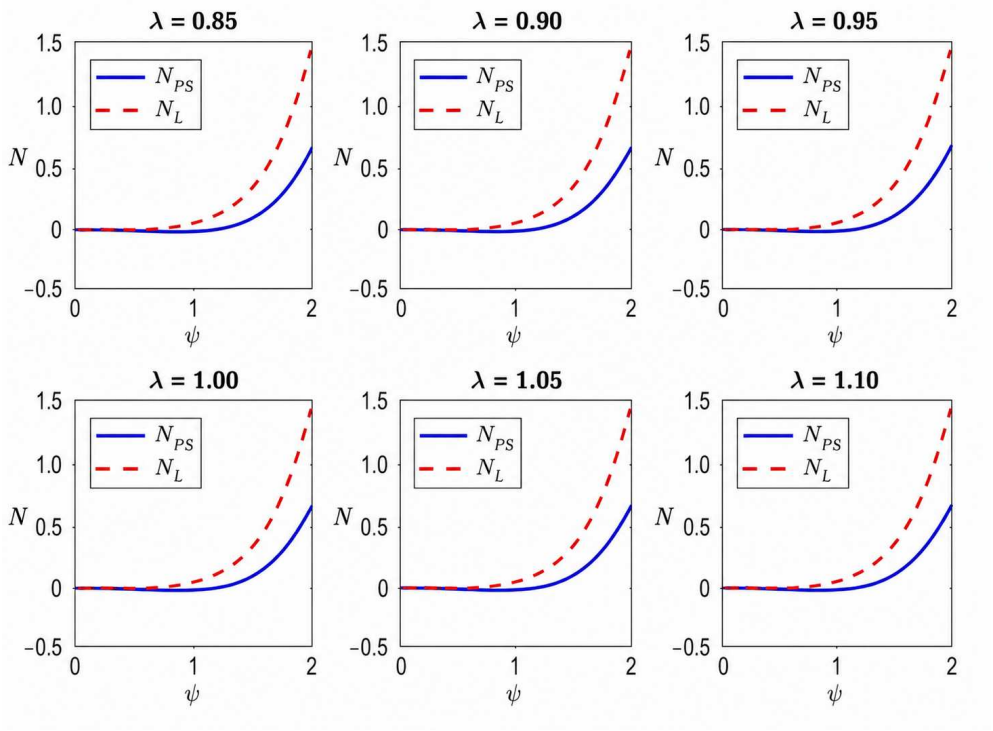



**Fig. 6** Evolution of the normal force $N$ with the twist angle $\psi$ for different values of $\lambda$: comparison between $N_{PS}$ and $N_L$ models and illustration of the Poynting effect

could have influenced the work reported in this article. In addition, they state that no funding was received for the conduct of this study. The authors appreciate the constructive comments and valuable suggestions provided by the reviewers of the members of the editorial board, which helped to improve the final version of this article.

# References

[1] Beda, T.: Modeling hyperelastic behavior of rubber: A novel invariant-based and a review of constitutive models. Journal of Polymer Science, Part B: Polymer Physics **45**(13), 1713–1732 (2007) https://doi.org/10.1002/polb.20928

[2] Nguessong, A.N., Beda, T., Peyraut, F.: A new based error approach to approximate the inverse langevin function. Rheologica Acta **53**(8), 585–591 (2014) https://doi.org/10.1007/s00397-014-0778-y

[3] Bien-aimé, L.K.M., Blaise, B.B., Beda, T.: Characterization of hyperelastic deformation behavior of rubber-like materials. SN Applied Sciences **2**(4) (2020) https://doi.org/10.1007/s42452-020-2355-6

[4] Bale, B., Blaise, Liman Madahan Kaoye Bien-aimé, Betchewe, G., Marckman, G.,

Beda, T.: A phenomenological expression of strain energy in large elastic deformations of isotropic materials. Iranian Polymer Journal **4**(0123456789) (2020) https://doi.org/10.1007/s13726-020-00816-6

[5] Bone Adji, Bale Baidi, B., Samon, J.B., Liman Kaoye Madahan, B.A., Beda Tibi: A hyperelastic model for mechanical characterization of human and animal skin behaviors. Applied Physics A: Materials Science and Processing **131**(10) (2025) https://doi.org/10.1007/s00339-025-08922-z

[6] Polignone, D.A., Horgan, C.O.: Pure torsion of compressible non-linearly elastic circular cylinders. Quarterly of Applied Mathematics **49**(3), 591–607 (1991) https://doi.org/10.1090/qam/1121689

[7] Chen, Z., Ren, H., Zhou, P., Fan, W.: Semi-analytical framework for nonlinear vibration analysis of hard-magnetic soft beams. International Journal of Mechanical Sciences **291-292** (2025) https://doi.org/10.1016/j.ijmecsci.2025.110149

[8] Chiaia, P., Pagani, A., Carrera, E.: Higher-order finite element modeling of biological tissues under large strain conditions. Journal of Sound and Vibration **633** (2026) https://doi.org/10.1016/j.jsv.2026.119737

[9] Haniszewski, T., Bucki, S., Margielewicz, J., Gąska, D., Kuang, Y., Litak, G.: Energy harvesting system with a hyperelastic mechanical vibration amplifier. Mechanical Systems and Signal Processing **224**, 112038 (2025) https://doi.org/10.1016/J.YMSSP.2024.112038

[10] Jing, J., Mao, X., Ding, H., Li, H., Chen, L.: Modeling and mechanism of vibration reduction of pipes by visco-hyperelastic materials. Applied Mathematics and Mechanics 2025 46:6 **46**(6), 1029–1048 (2025) https://doi.org/10.1007/S10483-025-3263-6

[11] Anssari-Benam, A., Horgan, C.O.: New constitutive models for the finite deformation of isotropic compressible elastomers. Mechanics of Materials **172** (2022) https://doi.org/10.1016/j.mechmat.2022.104403

[12] Kaoye, L., Bien-Aimé, M., Student, P., Blaise, B.B., Beda, T.: Comparison of Continuum Constitutive Hyperelastic Models based on Exponential Forms. Technical Report 7 (2019). www.ijisrt.com

[13] Beda, T., Chevalier, Y.: Non-linear approximation method by an approach in stages. Computational Mechanics **32**(3), 177–184 (2003) https://doi.org/10.1007/s00466-003-0473-9

[14] Blaise, B.B., Betchewe, G., Beda, T.: Optimization of the model of Ogden energy by the genetic algorithm method. Applied Rheology **29**(1), 21–29 (2019) https://doi.org/10.1515/arh-2019-0003

[15] Blaise, B.B., Betchewe, G., Beda, T.: Optimization of the model of Ogden energy by the genetic algorithm method. Applied Rheology **29**(1), 21–29 (2019) https://doi.org/10.1515/arh-2019-0003

[16] Ogden, R.W., Saccomandi, G., Sgura, I.: Fitting hyperelastic models to experimental data. Computational Mechanics **34**(6), 484–502 (2004) https://doi.org/10.1007/s00466-004-0593-y

[17] Treloar, L.R.G.: Stress-strain data for vulcanised rubber under various types of deformation. Transactions of the Faraday Society **40**(0), 59–70 (1944) https://doi.org/10.1039/TF9444000059

[18] Rivlin, R.S.: Large elastic deformations of isotropic materials IV. further developments of the general theory. Philosophical Transactions of the Royal Society of London. Series A, Mathematical and Physical Sciences **241**(835), 379–397 (1948) https://doi.org/10.1098/rsta.1948.0024

[19] Green, A.E., Shield, R.T.: Finite extension and torsion of cylinders. Philosophical Transactions of the Royal Society of London. Series A, Mathematical and Physical Sciences **244**(876), 47–86 (1951) https://doi.org/10.1098/rsta.1951.0015

[20] Gent, A.N., Hua, K.C.: Torsional instability of stretched rubber cylinders. International Journal of Non-Linear Mechanics **39**(3), 483–489 (2004) https://doi.org/10.1016/S0020-7462(02)00217-2

[21] Horgan, C.O., Murphy, J.G.: Extension and torsion of incompressible non-linearly elastic solid circular cylinders. Mathematics and Mechanics of Solids **16**(5), 482–491 (2011) https://doi.org/10.1177/1081286510387720

[22] Shang, Y., Fan, Q., Shang, L., Sun, Z., Xiao, G.: Modified genetic algorithm with simulated annealing applied to optimal load dispatch of the Three Gorges Hydropower Plant in China. Hydrological Sciences Journal **64**(9), 1129–1139 (2019) https://doi.org/10.1080/02626667.2019.1625052

[23] Anssari-Benam, A., Horgan, C.O.: Extension and torsion of rubber-like hollow and solid circular cylinders for incompressible isotropic hyperelastic materials with limiting chain extensibility **92**, 104443 (2022) https://doi.org/10.1016/j.euromechsol.2021.104443

[24] Anssari-Benam, A., Horgan, C.O.: Torsional instability of incompressible hyperelastic rubber-like solid circular cylinders with limiting chain extensibility. International Journal of Solids and Structures **238** (2022) https://doi.org/10.1016/j.ijsolstr.2021.111396

[25] Dya, T., Blaise, B.B., Betchewe, G., Bien-aimé, L.K.M., Beda, T., Alidou, M.: Characterization of pure torsion of a rubber-like cylinder using a hyperelastic model. European Physical Journal Plus **137**(5), 531 (2022) https://doi.org/10.

1140/epjp/s13360-022-02737-0

[26] Horgan, C.O., Murphy, J.G.: Pure torsion for incompressible hyperelastic materials of Valanis-Landel form **479**, 101–111 (2023)

[27] Bacciocchi, M., Tarantino, A.M.: Finite torsion of transversely isotropic compressible hyperelastic circular cylinders. International Journal of Mechanical Sciences **303**, 110582 (2025) https://doi.org/10.1016/j.ijmecsci.2025.110582

[28] Gent, A.N.: Extensibility of rubber under different types of deformation. Journal of Rheology **49**(1), 271–275 (2005) https://doi.org/10.1122/1.1835343

[29] Horgan, C.O., Saccomandi, G.: Simple Torsion of Isotropic, Hyperelastic, Incompressible Materials with Limiting Chain Extensibility. Journal of Elasticity **56**(2), 159–170 (1999) https://doi.org/10.1023/A:1007606909163

[30] Pucci, E., Saccomandi, G.: A note on the gent model for rubber-like materials. Rubber Chemistry and Technology **75**(5), 839–851 (2002) https://doi.org/10.5254/1.3547687

[31] Gornet, L., Marckmann, G., Desmorat, R., Charrier, P.: A new isotropic hyperelastic strain energy function in terms of invariants and its derivation into a pseudo-elastic model for Mullins effect: Application to finite element analysis. In: Constitutive Models for Rubber VII, pp. 265–271 (2011). https://doi.org/10.1201/b11687-49

[32] Blaise, B.B., Kaoye, L., Samon, B., Betchewe, G., Beda, T.: Characterization of the Preloaded Hyperelastic Materials Subjected to Linear Vibrations. Journal of Vibration Engineering and Technologies **12**(4), 6031–6041 (2024) https://doi.org/10.1007/s42417-023-01234-7

[33] Goldberg, D.E., Holland, J.H.: Genetic Algorithms in Search, Optimization, and Machine Learning David E. Goldberg The University of Alabama T. Machine Learning **3**(2), 95–99 (1979) https://doi.org/10.1007/BF01920603

[34] Elsayed, S.M., Sarker, R.A., Essam, D.L.: A new genetic algorithm for solving optimization problems. Engineering Applications of Artificial Intelligence **27**(C), 57–69 (2014) https://doi.org/10.1016/j.engappai.2013.09.013

[35] Rivlin, R.S., Saunders, D.W.: Large Elastic Deformations of Isotropic Materials. VII. Experiments on the Deformation of Rubber. Philosophical Transactions of the Royal Society A: Mathematical, Physical and Engineering Sciences **243**(865), 251–288 (1951) https://doi.org/10.1098/rsta.1951.0004

[36] Horgan, C.O., Murphy, J.G.: The effect of fiber-matrix interaction on the Poynting effect for torsion of fibrous soft biomaterials. Journal of the Mechanical Behavior of Biomedical Materials **118** (2021) https://doi.org/10.1016/j.jmbbm.

2021.104410

[37] Horgan, C.O., Vitral, E.: Further Results on Stretch Formulations of Simple Shear and Pure Torsion for Incompressible Isotropic Hyperelastic Materials. Journal of Elasticity 2023 153:2 **153**(2), 207–217 (2023) https://doi.org/10.1007/S10659-022-09980-7

[38] Vitral, E.: Stretch formulations and the Poynting effect in nonlinear elasticity. International Journal of Non-Linear Mechanics **148** (2023) https://doi.org/10.1016/j.ijnonlinmec.2022.104293

[39] Thiel, C., Voss, J., Martin, R.J., Neff, P.: Shear, pure and simple. International Journal of Non-Linear Mechanics **112**, 57–72 (2019) https://doi.org/10.1016/j.ijnonlinmec.2018.10.002 arXiv:1806.07749

[40] Askari-sedeh, M., Baghani, M.: On the extension-torsion of short hyperelastic tubes of axially functionally-graded materials. Engineering Structures **301** (2024) https://doi.org/10.1016/j.engstruct.2023.117344

[41] Horgan, C.O.: Pure Torsion for Stretch-Based Constitutive Models for Incompressible Isotropic Hyperelastic Soft Materials. Journal of Elasticity 2024 156:1 **156**(1), 237–254 (2024) https://doi.org/10.1007/S10659-024-10048-X

[42] Bacciocchi, M., Tarantino, A.M.: Finite torsion of transversely isotropic compressible hyperelastic circular cylinders. International Journal of Mechanical Sciences **303**, 110582 (2025) https://doi.org/10.1016/J.IJMECSCI.2025.110582

[43] Falope, F.O., Lanzoni, L., Tarantino, A.M.: Experiments on the finite torsion of nearly incompressible rubber-like materials: Nonlinear effects, analytic modeling and rubber characterization. International Journal of Engineering Science **211**, 104254 (2025) https://doi.org/10.1016/j.ijengsci.2025.104254

[44] Lectez, A.S., Verron, E., Huneau, B.: How to identify a hyperelastic constitutive equation for rubber-like materials with multiaxial tension-torsion experiments. International Journal of Non-Linear Mechanics **65**, 260–270 (2014) https://doi.org/10.1016/j.ijnonlinmec.2014.06.007

[45] Blaise, B.B., Bien-aimé, L.K.M., Betchewe, G., Marckman, G., Beda, T.: A phenomenological expression of strain energy in large elastic deformations of isotropic materials. Iranian Polymer Journal **4**, 1–9 (2020) https://doi.org/10.1007/s13726-020-00816-6

[46] Silva, M.X., Silva, F.T., Galvão, B.R.L., Braga, J.P., Belchior, J.C.: A genetic algorithm survey on closed-shell atomic nitrogen clusters employing a quantum chemical approach. Journal of Molecular Modeling **24**(8) (2018) https://doi.org/10.1007/s00894-018-3724-6

[47] Gent, A.N., Thomas, A.G.: Forms for the stored (strain) energy function for vulcanized rubber. Journal of Polymer Science **28**(118), 625–628 (1958) https://doi.org/10.1002/pol.1958.1202811814

[48] Gent, A.N.: A new constitutive relation for rubber. Rubber Chem. Technol. **69**(1), 59–61 (1996) https://doi.org/10.5254/1.3538357

[49] Dya, T., Blaise, B.B., Betchewe, G., Bien-aimé, L.K.M., Beda, T., Alidou, M.: Characterization of pure torsion of a rubber-like cylinder using a hyperelastic model. European Physical Journal Plus **137**(5) (2022) https://doi.org/10.1140/epjp/s13360-022-02737-0

[50] Wang, D., Wu, M.S.: Poynting and axial force-twist effects in nonlinear elastic mono- and bi-layered cylinders: Torsion, axial and combined loadings. International Journal of Solids and Structures **51**(5), 1003–1019 (2014) https://doi.org/10.1016/j.ijsolstr.2013.11.027

[51] Liu, H., Liu, L., Liu, D.: The mechanics and morphology evolutions in stretched ribbons under torsion: A 3D phase diagram. International Journal of Mechanical Sciences **285** (2025) https://doi.org/10.1016/j.ijmecsci.2024.109786

[52] Ogden, R.W.: Biaxial deformation of rubber-like solids: comparison of theory and experiment. Journal of Physics D: Applied Physics **12**(9), 1463–1472 (1979) https://doi.org/10.1088/0022-3727/12/9/008

[53] Arruda, E.M., Boyce, M.C.: A three-dimensional constitutive model for the large stretch behavior of rubber elastic materials. Journal of the Mechanics and Physics of Solids **41**(2), 389–412 (1993) https://doi.org/10.1016/0022-5096(93)90013-6

[54] Mullins, L.: Softening of Rubber by Deformation. Rubber Chemistry and Technology **42**(1), 339–362 (2011) https://doi.org/10.5254/1.3539210

[55] Horgan, C.O., Murphy, J.G.: Poynting and reverse Poynting effects in soft materials. Soft Matter **13**(28), 4916–4923 (2017) https://doi.org/10.1039/c7sm00992e

[56] Areias, P., Rabczuk, T., Vaz, M.F., Sardinha, M., Leite, M.: A consistent algorithm for finite-strain visco-hyperelasticity and visco-plasticity of amorphous polymers. Computer Methods in Applied Mechanics and Engineering **400**, 115528 (2022) https://doi.org/10.1016/j.cma.2022.115528

[57] Zhang, X., Zhang, S., Zhang, H., Liu, C., Zhou, Y., Dong, C., Gao, X., Wang, F., Song, Y.: A hyperelastic model considering the coupling of shear-compression for the forming simulation of 3D orthogonal composite preforms. Composites Science and Technology **258**, 110884 (2024) https://doi.org/10.1016/j.compscitech.2024.110884